Non-small cell lung cancer is characterized by dramatic changes in phospholipid profiles

IJC
International Journal of Cancer

Non-small cell lung cancer is characterized by dramatic changes in phospholipid profiles

Eyra Marien[1], Michael Meister[2,3], Thomas Muley[2,3], Steffen Fieuws[4], Sergio Bordel[5], Rita Derua[6], Jeffrey Spraggins[7], Raf Van de Plas[7,8], Jonas Dehairs[1], Jens Wouters[1], Muralidhararao Bagadi[1], Hendrik Dienemann[3,9], Michael Thomas[3,10], Philipp A. Schnabel[3,11], Richard M. Caprioli[7], Etienne Waelkens[6] and Johannes V. Swinnen[1]

[1] Department of Oncology, Laboratory of Lipid Metabolism and Cancer, KU Leuven—University of Leuven, Leuven, Belgium
[2] Thoraxklinik at University Hospital Heidelberg, Translational Research Unit, Heidelberg, Germany
[3] TLRC-H – Translational Lung Research Center Heidelberg, Member of the German Center for Lung Research, Heidelberg, Germany
[4] Department of Public Health and Primary Care, I-Biostat KU Leuven—University of Leuven and Universiteit Hasselt, Leuven, Belgium
[5] Department of Chemical and Biological Engineering, Systems Biology Group, Chalmers University of Technology, Gothenburg, Sweden
[6] Department of Cellular and Molecular Medicine, Laboratory of Protein Phosphorylation and Proteomics, KU Leuven – University of Leuven, Leuven, Belgium
[7] Department of Biochemistry and Mass Spectrometry Research Center, Vanderbilt University Medical Center, Nashville, TN
[8] Delft University of Technology, Delft Center for Systems and Control, CD Delft, The Netherlands
[9] Department of Surgery, Thoraxklinik at University Hospital Heidelberg, Heidelberg, Germany
[10] Department of Thoracic Oncology, Thoraxklinik at University Hospital Heidelberg, Heidelberg, Germany
[11] University Hospital Heidelberg, Institute of Pathology, Heidelberg, Germany

Non-small cell lung cancer (NSCLC) is the leading cause of cancer death globally. To develop better diagnostics and more effective treatments, research in the past decades has focused on identification of molecular changes in the genome, transcriptome, proteome, and more recently also the metabolome. Phospholipids, which nevertheless play a central role in cell functioning, remain poorly explored. Here, using a mass spectrometry (MS)-based phospholipidomics approach, we profiled 179 phospholipid species in malignant and matched non-malignant lung tissue of 162 NSCLC patients (73 in a discovery cohort and 89 in a validation cohort). We identified 91 phospholipid species that were differentially expressed in cancer versus non-malignant tissues. Most prominent changes included a decrease in sphingomyelins (SMs) and an increase in specific phosphatidylinositols (PIs). Also a decrease in multiple phosphatidylserines (PSs) was observed, along with an increase in several phosphatidylethanolamine (PE) and phosphatidylcholine (PC) species, particularly those with 40 or 42 carbon atoms in both fatty acyl chains together. 2D-imaging MS of the most differentially expressed phospholipids confirmed their differential abundance in cancer cells. We identified lipid markers that can discriminate tumor versus normal tissue and different NSCLC subtypes with an AUC (area under the ROC curve) of 0.999 and 0.885, respectively. In conclusion, using both shotgun and

Key words: non-small cell lung cancer, lipidomics, phospholipids, mass spectrometry, 2D-imaging MS

Abbreviations: AD: adenocarcinoma; AUC: area under the ROC-curve; CI: confidence interval; CPE: concordance probability estimate; CV: cross-validation; ESI-MS/MS: electrospray ionization tandem mass spectrometry; FDR: false discovery rate; HR: hazard ratio; LDA: linear discriminant analysis; MALDI: matrix-assisted laser desorption/ionization; MRM: multiple reaction monitoring; MS: mass spectrometry; NSCLC: non-small cell lung cancer; PC: phosphatidylcholine; PE: phosphatidylethanolamine; PI: phosphatisylinositol; PCA: principal component analysis; PS: phosphatidylserine; SCC: squamous cell carcinoma; SM: sphingomyelin

Additional Supporting Information may be found in the online version of this article.

Grant sponsor: EU FP7 (to J.Sw., M.M., T.M. and M.T.); **Grant number:** Canceralia EU-259737; **Grant sponsor:** Research Foundation-Flanders (FWO) (to J.Sw.); **Grant number:** G.0691.12; **Grant sponsor:** KU Leuven (to J.Sw.); **Grant number:** GOA/11/2009; **Grant sponsor:** Foundation Fournier Majoie (FFM) (to J.Sw.); **Grant sponsor:** Stichting tegen Kanker (to J.Sw.); **Grant number:** F/2014/324; **Grant sponsor:** Agency for Innovation by Science and Technology IWT-Flanders (to E.M. and J.D.; recipients of a fellowship); **Grant sponsor:** Olle Engkvist foundation (Sweden) (to S.B.); **Grant sponsor:** National Institutes of Health (to J.Sp., R.V. and R.M.C.); **Grant numbers:** NIH/NIGMS R01 GM058008-14 and NIH/NIGMS P41 GM103391-03

DOI: 10.1002/ijc.29517
History: Received 3 Nov 2014; Accepted 5 Mar 2015; Online 18 Mar 2015

Correspondence to: Johannes V. Swinnen, Laboratory of Lipid Metabolism and Cancer, KU Leuven, Gasthuisberg, O&N I Herestraat 49 - box 902, B-3000 Leuven, Belgium, Tel.: +32-16-330533, Fax: +32-16-330718, E-mail: johan.swinnen@med.kuleuven.be

2D-imaging lipidomics analysis, we uncovered a hitherto unrecognized alteration in phospholipid profiles in NSCLC. These changes may have important biological implications and may have significant potential for biomarker development.

What's new?

Cellular membranes are subject to extensive modification in cancer, often with marked alterations in phospholipid metabolism. The extent and nature of those changes are not fully known, however, particularly for non-small cell lung cancer (NSCLC). In this study, lipidomics analysis of phospholipid profiles uncovered dramatic differences between NSCLC and normal lung tissue. The differences were confirmed via 2D-imaging lipidomics in tissue sections. Lipid markers capable of discriminating between tumor and normal tissue and between different NSCLC subtypes were identified. The observed alterations in NSCLC phospholipid profiles may be biologically significant.

With more than 1.6 million victims per year, lung cancer is the deadliest of all cancers in the world.[1] Particularly non-small cell lung cancer (NSCLC) is very prevalent and accounts for 80% of all lung cancer cases. One of the key problems in the management of NSCLC is the high failure rate of existing treatments, urging the need for new molecular biomarkers and novel therapeutic targets. Most efforts towards this molecular characterization have been carried out at the level of the genome, transcriptome, proteome, and lately also the metabolome.[2–7] The lipidome and particularly the phospholipidome remain, however, poorly explored. Nevertheless, phospholipids play a central role in cell biology. Functioning as the main building blocks of cellular membranes, phospholipids are essential to build up barriers that protect the cell from its surroundings and that compartmentalize and control numerous cellular processes. These molecules, or derivatives thereof, also act as important signaling molecules that regulate key cellular responses or play specialized roles for instance as lung surfactants. As phospholipids can have different headgroups and are typically composed of multiple fatty acyl chains that can differ in both their length and in their degree of unsaturation, there is a huge variety of phospholipid species. As each species has unique properties and can differentially affect the folding, structure and functioning of membrane proteins,[8] the specific lipid composition of membranes determines the physical and functional characteristics of membranes, and hence has major biological implications. Not surprisingly, several alterations in phospholipid metabolism have been observed in cancer cells. It has been long recognized that cancer cells require more membranes for rapid cell proliferation and, therefore, often show a brisk synthesis of fatty acids that are used as building blocks for phospholipids.[9,10] This is enabled by a marked overexpression and activation of key lipogenic enzymes including fatty acid synthase.[11] Also enzymes involved in the metabolism, hydrolysis and remodeling of fatty acyl chains, including stearoyl CoA-desaturase and several phospholipases are often aberrantly expressed in cancer tissue.[12,13] Also in NSCLC, several of these enzymes are affected.[14,15] Nevertheless, it remains unknown to what extent phospholipid profiles are altered in NSCLC tissue. As a first step in the elucidation of alterations in phospholipid metabolism in lung cancer and to explore the potential of phospholipids as future biomarkers for lung cancer, we have used a shotgun electrospray ionization tandem mass spectrometry (ESI-MS/MS) approach to study tumor-associated changes of common phospholipids in NSCLC. Using this approach, along with 2D-imaging MS[16] of selected phospholipid species in tissue sections we demonstrate that lung cancer tissue has a dramatically different phospholipid composition compared to normal tissue. These findings are of seminal importance for the further exploration of altered lipid metabolism in lung cancer and may hold significant potential for the development of biomarkers.

Material and Methods

Clinical tissue specimens

Tumor and matched distant ($>$ 5 cm) normal lung tissue samples were collected from NSCLC patients undergoing surgery and were snap-frozen in liquid nitrogen within 30 min after resection and stored at -80°C. Samples from 73 patients were used as a discovery set and samples from 89 patients were used to validate the results (referred to as the validation set). Selection was based on Stage (I–IIIa), complete resection of the tumor during surgery, absence of prior malignancy, viable tumor content of $\geq$50%, and macroscopically confirmed absence of tumor in matched normal tissue. The characteristics of the patients are given in Supporting Information Table S1. All patients gave their informed consent following the guidelines of the 2008 revision of the declaration of Helsinki and the local Ethics Committee of the Medical Faculty Heidelberg. Approval to perform lipidomics analysis on clinical samples was obtained from the local Ethical Committee of the KU Leuven.

Analysis of intact phospholipid species by electrospray ionization tandem mass spectrometry

Tissue was homogenized in PBS using 0.9–2.0 stainless steel beads in a bullet blender (Next Advance) and 700 µl of this homogenate was mixed with 800 µl 1 N HCl:CH_3OH 1:8 (v/v), 900 µl $CHCl_3$ and 200 µg/ml of the antioxidant 2,6-di-tert-butyl-4-

methylphenol (BHT; Sigma Aldrich). The organic fraction was evaporated using a Savant Speedvac spd111v (Thermo Fisher Scientific) at room temperature and the remaining lipid pellet was stored at −20°C under argon. Just before mass spectrometry analysis, lipid pellets were reconstituted in running solution (CH_3OH:$CHCl_3$:NH_4OH; 90:10:1.25; v/v/v). Phospholipid species were analyzed by electrospray ionization tandem mass spectrometry (ESI-MS/MS) on a hybrid triple quadrupole/linear ion trap mass spectrometer (4000 QTRAP system; AB SCIEX) equipped with a TriVersa NanoMate (Advion Biosciences) robotic nanosource for automated sample injection and spraying. Phospholipid profiling was executed by (positive or negative) precursor ion or neutral loss scanning at a collision energy of 50 eV/45 eV, 35 eV, −35 eV and −60 eV for precursor 184 [sphingomyelin (SM)/phosphatidylcholine (PC)], neutral loss 141 [phosphatidylethanolamine (PE)], neutral loss 87 [phosphatidylserine (PS)] and precursor 241 [phosphatidylinositol (PI)], respectively. Phospholipid quantification was performed by multiple reaction monitoring (MRM), the transitions being based on the neutral losses or the typical product ions as described above. Lipid standards PC25:0, PC43:6, SM30:1, PE25:0, PE43:6, PI25:0, PI31:1, PI43:6, PS25:0, PS31:1 and PS37:4 (Avanti Polar Lipids) were added based on the amount of DNA of the original sample. Typically, a 3 min period of signal averaging was used for each spectrum. The data were corrected for carbon isotope effects and chain length and analyzed using in house-developed software (RALP). Only the phospholipid species displaying an intensity of at least 5 times the blank value were taken into account and are summarized in Supporting Information Table S2. In order to quantify the total amount of phospholipids in a phospholipid class, we summed the abundances of individually measured species within the phospholipid class. Data were normalized based on the amount of DNA. Clustering analysis was carried out using an average linkage-clustering algorithm (Spearman rank correlation) in the Cluster 3.0 software. The clustering results were visualized using the Java TreeView 1.1.5 software.

2D-imaging MS

Image experiments were performed using a 15T Bruker MALDI (matrix-assisted laser desorption/ionization) FTICR mass spectrometer (Bruker Daltonics) both in positive ion mode (SM) and in negative ion mode (PI) to screen for different lipid species. Sections of 10 μm from the frozen lung tissue were obtained using a cryostat and mounted onto indium tin oxide (ITO)-coated glass slides. 2,6-dihydroxyacetophenone (DHA; Sigma Aldrich) matrix was applied by sublimation[17] for both positive and negative ion mode analysis. The instrument is equipped with an Apollo II dual MALDI/ESI ion source and a Smartbeam II 2 kHz Nd:YAG (355 nm) laser. All images were collected using the small laser setting (∼50 μm) with a pixel spacing of 100 μm in both *x* and *y* directions. For positive mode analysis, data was collected from *m/z* 500–2,000 with a resolving power of ∼200,000 at *m/z* 734.6 and <1 ppm mass accuracy. In negative mode, a range of *m/z* 300–2,000 was acquired with a resolving power of ∼350,000 at *m/z* 744.6 and <1 ppm mass accuracy. FlexImaging (Bruker Daltonics) was used to visualize the ion images.

Statistical analysis

Statistical analysis was carried out in GraphPad Prism (Version 6.0c of the GraphPad system for Mac) and SAS software (Version 9.2 of the SAS system for Windows). Spearman correlations were used to evaluate the relation between the abundances of the major phospholipid classes. The abundance of the major phospholipid classes and the specific phospholipid species were compared between tumor and normal tissue with Mann-Whitney U tests (MWU). For the specific phospholipid species, a Benjamini Hochberg false discovery rate (FDR) correction for multiple testing[18] was applied. The discriminative ability was quantified with the area under the ROC-curve (AUC). We deliberately did not use the paired character (tumor and normal tissue from the same patient) of the data in the statistical evaluations, since in a practical setting of clinical biomarker analysis, normal tissue will typically not be available. Analyses have been performed on a first set of 73 patients (the discovery set) and conclusions were verified on an additional set of 89 patients (the validation set). Hazard ratios (HR) were reported for the associations between lipid abundance and survival outcome variables (overall survival, recurrence and metastasis) and the concordance probability estimate (CPE) is reported to quantify the discriminative ability.[19] To increase the power of the analysis, relations with clinical outcome were studied in the total dataset of 162 patients (both datasets together). Finally, a principal component analysis (PCA) has been performed on the phospholipid profiles, followed by linear discriminant analysis (LDA) to distinguish NSCLC *versus* normal tissue and the clinical subtypes adenocarcinoma (AD) *versus* squamous cell carcinoma (SCC) based on the PCA scores. A cross-validation procedure was applied for the discovery set by splitting the data 1,000 times at random into a training (80%) and test (20%) set. Each discriminating model was learned from a training set and evaluated in the corresponding test set. The mean performance (over the 1,000 sample partitions) was compared to the (overoptimistic) observed performance, that is, the result on the full dataset (100%). The AUC based on the cross-validation is referred to as AUC_{CV}. The LDA creates a new variable, that is, a linear combination of the principal component scores (this new variable is the canonical variable). The result of the PCA-LDA on the discovery set (more specifically, the canonical score from the LDA based on a specific number of principal component scores) was validated on the data of the validation set using the weights (to construct the PCA scores and the canonical score) obtained from the analysis of the discovery set.

Results

NSCLC tissues show a different phospholipid profile compared to normal tissues

To examine potential alterations in phospholipid profiles in NSCLC tissues compared to normal lung tissues we initially

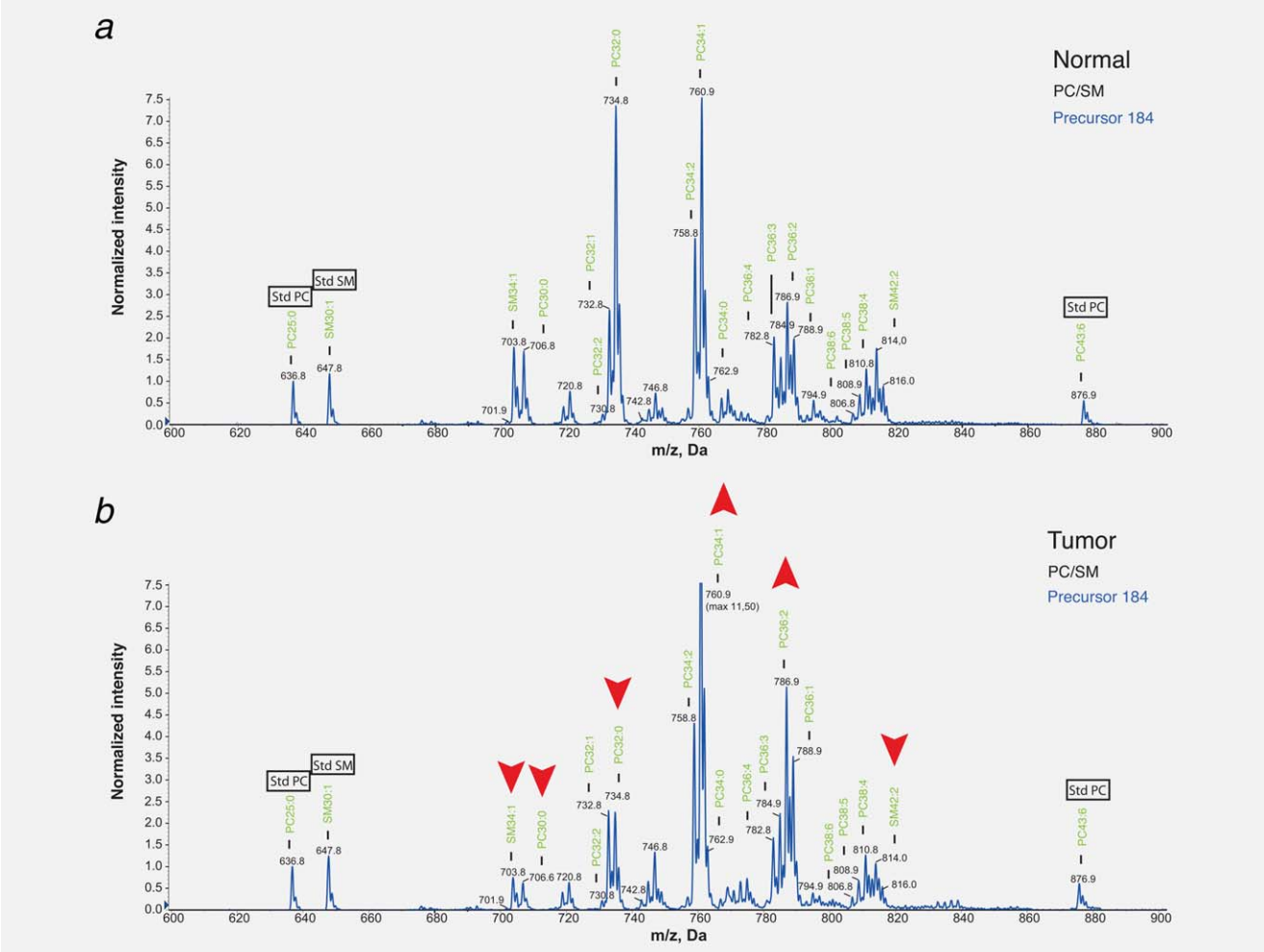

Figure 1. Precursor ion scan of phosphocholine-containing phospholipid species in tumor *versus* matching normal tissue of a representative SCC patient. Lipids were extracted from tumor and normal tissue of a representative SCC patient and were subjected to positive ion ESI-MS/MS analysis in precursor ion *m/z* 184 scanning mode for the specific detection of phosphocholine-containing phospholipid species. Std refers to the lipid standards. Intensities were normalized to the peak height of standard PC25:0. Red arrows indicate striking differences between the spectra of (*b*) tumor and (*a*) matched normal tissue. Major lipid species are annotated.

analyzed cancer and matching normal tissue from 73 NSCLC patients. This discovery set encompassed the three major NSCLC subtypes and consisted of 41 adenocarcinomas (ADs), 30 squamous cell carcinomas (SCCs) and two large cell carcinomas. Lipid extracts were prepared and subjected to an ESI-MS/MS based phospholipidomics approach enabling the identification and relative quantification of intact phospholipid species from five major phospholipid headgroup classes: phosphatidylcholine (PC), phosphatdidylethanolamine (PE), phosphatidylinositol (PI), phosphatidylserine (PS) and sphingomyelin (SM). From a preselected list of 241 commonly occurring phospholipid species, 179 ion species were detected at sufficient levels for further quantification. These included 51 PC, 43 PE, 45 PS, 33 PI and 7 SM molecular species (Supporting Information Table S2). Interestingly, remarkable changes were observed in the mass spectra of tumor *versus* matched normal tissue as illustrated for a representative SCC patient in Figure 1. Comparison of phospholipid changes in the entire set of 73 patients revealed recurrent changes in the majority of patients (Fig. 2). Most prominent changes included an increase in PI38:3, PI40:3 and PI38:2 and a decrease in SM40:1, SM42:1 and SM36:1 in tumor compared to matched normal tissue. Moreover a decrease in multiple PS species was observed, as well as an increase in several PEs and PCs with 40 or 42 carbon atoms in both fatty acyl chains together. To confirm that these lipid alterations in whole tissue extracts reflect changes in the abundance in cancer cells and not merely reflect changes in cell type composition, we performed 2D-imaging MS of a selection of some of the most differentially expressed phospholipids (PI38:3, PI40:3, PI38:2, SM40:1, SM42:1 and SM36:1) in tissue sections containing both cancer and adjacent non-malignant tissue. Consistent with the observed alterations in these lipid species in lipid extracts, a substantial increase was observed in the selected PI species in cancer regions of the tissues sections compared to adjacent non-

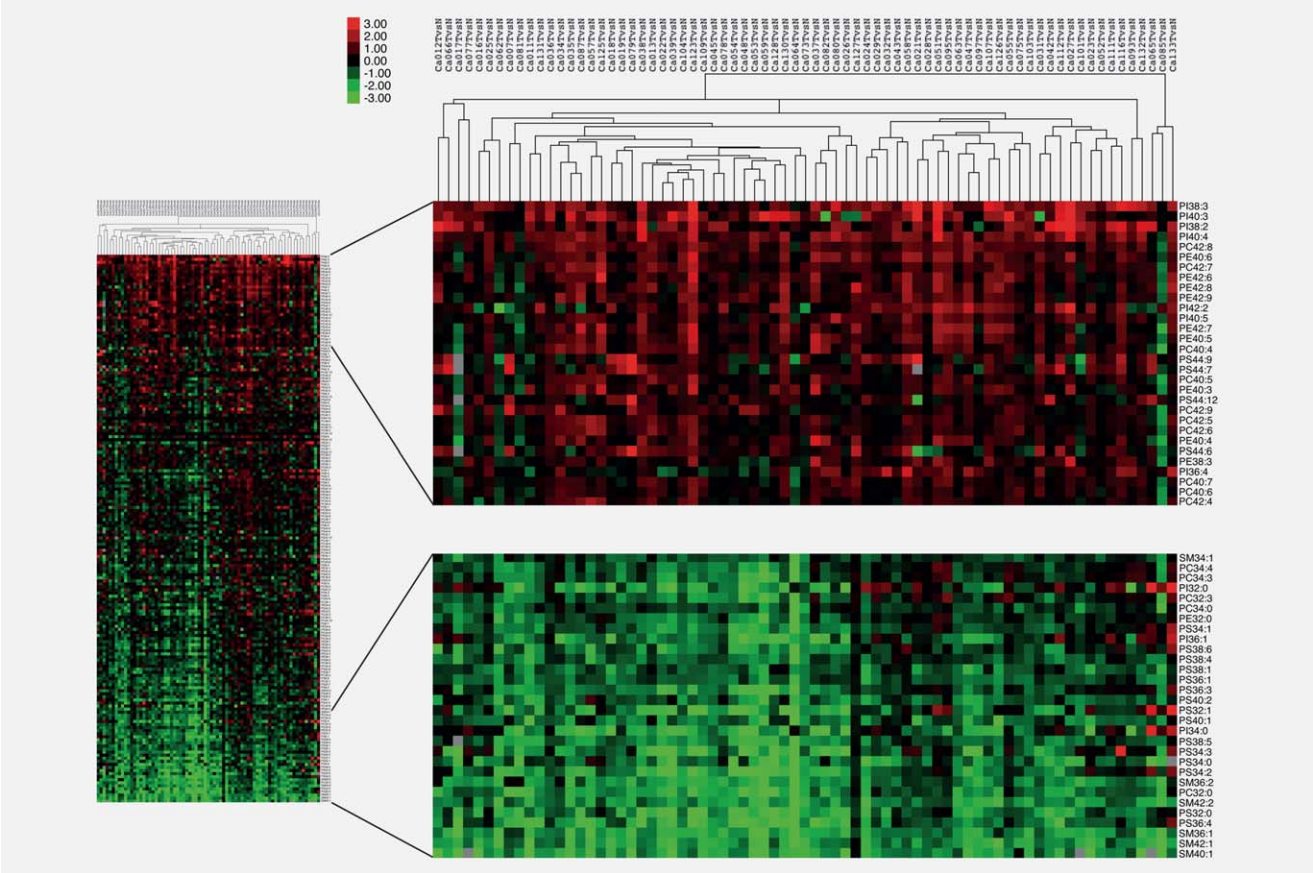

Figure 2. Changes in absolute abundance of phospholipid species in NSCLC *versus* matched normal lung tissue. Lipids were extracted from tumor and matched normal tissue from 73 NSCLC patients (discovery set) and were measured using ESI-MS/MS operated in MRM mode. Green squares indicate a decrease in absolute phospholipid abundance while red squares represent an increase as indicated by the scale bar (Log2 of the ratio). Grey squares indicate missing values. Phospholipid species are ranked based on their degree of up or down-regulation in tumor compared to normal tissue. Average linkage was used as clustering method. Panels on the right show an enlarged view of the top 30 up and downregulated lipid species.

malignant tissue (Fig. 3 and Supporting Information Fig. S1). Interestingly, the increased intensity of these PI molecular species in tumor areas was confined to the tumor cell nests and was not observed in the tumor stroma. SM species showed a decreased signal in tumor cell nests (Fig. 3 and Supporting Information Fig. S1). These findings confirmed that the observed changes in lipid profiles are caused by their differential expression in the cancer cells themselves and do not merely reflect changes in cell type composition.

Identification of phospholipid signatures that statistically discriminate between NSCLC and normal tissues

When tumor and normal tissues from the discovery set were compared independently from each other, statistical analysis of the abundances of individual phospholipid ion species revealed that 108 of the 179 measured species were significantly ($p < 0.05$, FDR) discriminative between tumor and normal tissue. To validate these findings we analyzed an additional 89 NSCLC tissues of which 44 ADs, 39 SCCs and 6 large. In this validation set, 91 species from the discovery set were confirmed to significantly ($p < 0.05$, FDR) discriminate tumor from normal tissue (Supporting Information Table S3). For 19 and 45 individual validated phospholipid species, the AUC was at least 0.90 and 0.80, respectively, in the discovery set. In Table 1 the 20 most discriminative species based on their AUC are given. The highest ranked species belonged to the phospholipid class SM (SM36:1, SM42:2, SM42:1, SM40:1, SM36:2 and SM34:1). Besides SM, several PS species (PS32:0, PS36:4, PS36:1, PS40:2, PS38:1, PS34:0, PS40:1, PS38:5, PS34:2 and PS38:4) were among the 20 highest ranked and validated species that could significantly differentiate tumor from normal tissue. Also, PI38:3, the phospholipid species that was increased most in NSCLC tissue (Fig. 2), is among the top 20 discriminative species.

Given the high discriminative ability of individual phospholipid species, it is not surprising that the (cross-validated) discriminative ability of a signature based on a principle component analysis (PCA) followed by a linear discriminant analysis (LDA) on a small number of principal component

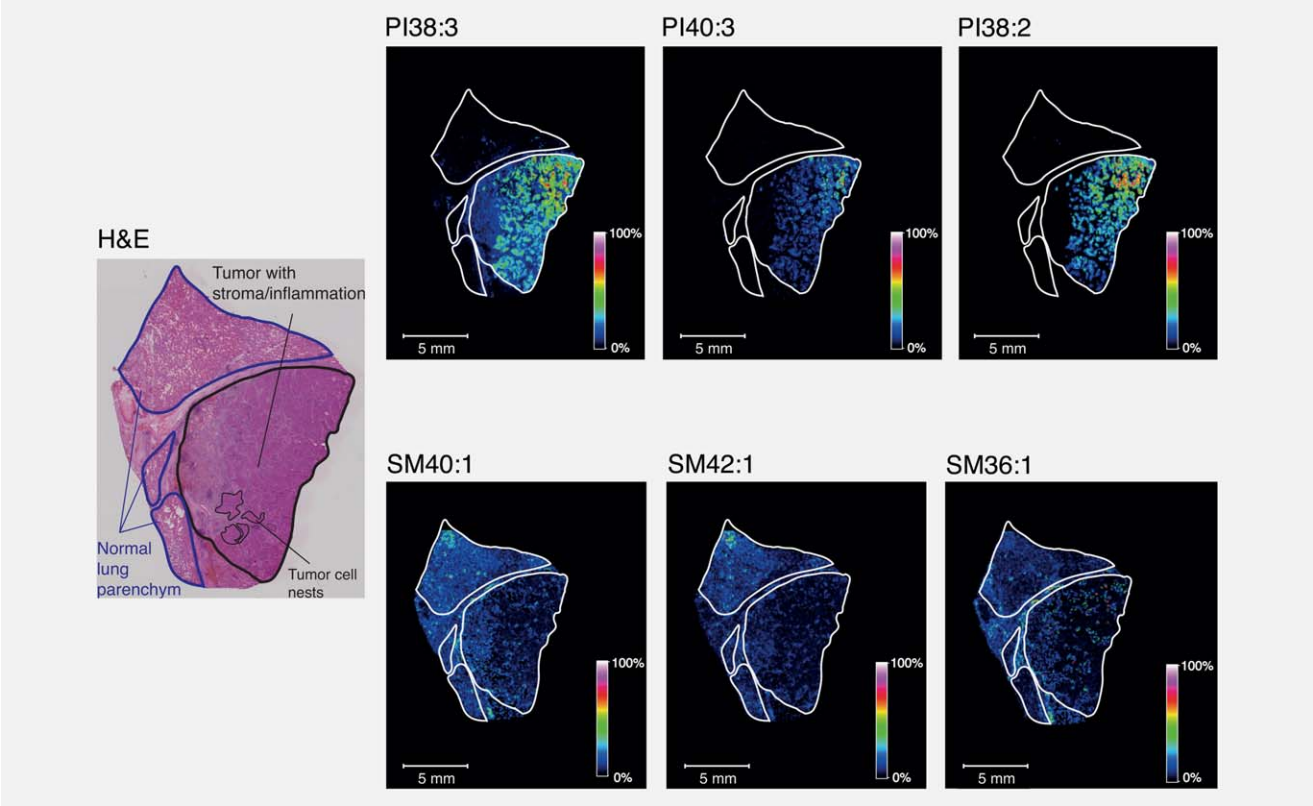

Figure 3. 2D-Imaging MS of the most differentially expressed phospholipids in a representative SCC and adjacent non-malignant tissue. Ion images of the selected molecular ions PI38:3 (*m/z* 887.5658 0.35 ppm), PI40:3 (*m/z* 915.5972 0.42 ppm), PI38:2 (*m/z* 889.5818 0.68 ppm), SM40:1 (*m/z* 787.6696 1.0 ppm), SM42:1 (*m/z* 815.7008 0.94 ppm) and SM36:1 (*m/z* 731.6069 1.0 ppm) are shown. Color intensities vary between 0 and 100% as indicated by the scale bars. H&E staining of a next tissue section is shown. Normal tissue, tumor tissue with stroma/inflammation, and tumor cell nests are indicated. Note that not all tumor cell nests are indicated, but some are circled as examples.

scores ($N = 5$; Supporting Information Fig. S2*a*) is maximal ($AUC_{CV} = 1.000$; discovery set). Moreover, the discriminative ability of the signature based on the PCA-LDA in the discovery set using 5 principal component scores was confirmed in the validation set (AUC = 0.999; Figs. 4*a* and 4*b*). Using 0.5 as cut-off for the posterior probability, all NSCLC tissues are correctly classified and only 3.4% of the normal tissues are misclassified.

Consistent with our observation that several phospholipid species of a specific headgroup class were similarly affected, analysis of total headgroup classes by summing all individually measured lipids of a particular class, revealed a marked overall decrease in the abundance of PC, PS and SM in the discovery set as illustrated in Supporting Information Figs. S3*a* and S3*b*. The abundances of both PS and SM were strongly correlated in both tumor and normal tissues (Supporting Information Figure S3*c*) and their correlation was the strongest correlation observed between any pair of phospholipid headgroup classes (Fig. S3*c*). Similar to the discovery set, tumor tissue of the validation set showed a significant overall decrease of PC (decrease of 19.8%; $p < 0.0001$), PS (decrease of 38.5%; $p < 0.0001$) and SM (decrease of 47.9%; $p < 0.0001$) (Figs. 4*c* and 4*d*). Moreover, the abundances of PS and SM were correlated (Fig. 4*e*) and their correlation coefficient was equal to 0.921 (SM *vs.* PS; $p < 0.0001$). The results of the validation set thus largely corroborate the results of the discovery set.

Phospholipid profiles can differentiate NSCLC subtypes

To explore to what extent the phospholipid content is different in the various NSCLC subtypes and can discriminate tumor subtypes, statistical analysis of the abundances of individual phospholipid ion species was performed in AD and SCC (Supporting Information Table S4). In contrast to the discrimination between NSCLC and normal tissues, individual species had lower ability to distinguish AD from SCC and we therefore combined abundances of different phospholipids by performing a PCA followed by LDA. When applied to the discovery set, lipid profiles were identified that could distinguish AD and SCC tumor types using 12 principal component scores (Supporting Information Fig. S2*b*; $AUC_{CV} = 0.846$). Moreover, the result of the PCA-LDA on the discovery set was confirmed in the validation set (AUC=0.885; Figs. 5*a* and 5*b*).

Relation between phospholipid abundance and overall survival, recurrence and metastasis

Finally, we also explored potential correlations of phospholipid profiles with clinical outcomes. The 10 best-ranked

Table 1. The top-20 species discriminating in the discovery set between NSCLC and normal tissue, and their performance in the validation set

		Discovery set		Validation set	
Rank	Species	AUC (95%CI)	*p* values (FDR)	AUC (95%CI)	*p* value (FDR)
1	SM36:1	1.000 (0.999;1.000)	<0.0001	0.984 (0.968;1.000)	<0.0001
2	SM42:2	1.000 (0.999;1.000)	<0.0001	0.963 (0.933;0.994)	<0.0001
3	SM42:1	0.995 (0.990;1.000)	<0.0001	0.973 (0.954;0.993)	<0.0001
4	SM40:1	0.993 (0.982;1.000)	<0.0001	0.938 (0.899;0.976)	<0.0001
5	SM36:2	0.971 (0.940;1.000)	<0.0001	0.957 (0.924;0.989)	<0.0001
6	PI38:3	0.969 (0.946;0.992)	<0.0001	0.956 (0.922;0.990)	<0.0001
7	PC32:0	0.963 (0.934;0.992)	<0.0001	0.954 (0.929;0.980)	<0.0001
8	PS32:0	0.961 (0.935;0.987)	<0.0001	0.945 (0.910;0.979)	<0.0001
9	PS36:4	0.949 (0.911;0.986)	<0.0001	0.944 (0.911;0.978)	<0.0001
10	PI40:4	0.943 (0.905;0.982)	<0.0001	0.910 (0.866;0.955)	<0.0001
11	PS36:1	0.942 (0.901;0.983)	<0.0001	0.924 (0.883;0.965)	<0.0001
12	PS40:2	0.940 (0.902;0.979)	<0.0001	0.894 (0.842;0.945)	<0.0001
13	PS38:1	0.938 (0.899;0.978)	<0.0001	0.881 (0.829;0.932)	<0.0001
14	PS34:0	0.934 (0.891;0.976)	<0.0001	0.894 (0.846;0.943)	<0.0001
15	PC42:8	0.929 (0.885;0.974)	<0.0001	0.791 (0.726;0.857)	<0.0001
16	PS40:1	0.929 (0.884;0.973)	<0.0001	0.905 (0.859;0.951)	<0.0001
17	SM34:1	0.921 (0.878;0.965)	<0.0001	0.794 (0.726;0.863)	<0.0001
18	PS38:5	0.917 (0.871;0.963)	<0.0001	0.930 (0.892;0.968)	<0.0001
19	PS34:2	0.912 (0.858;0.966)	<0.0001	0.885 (0.833;0.937)	<0.0001
20	PS38:4	0.895 (0.839;0.951)	<0.0001	0.911 (0.865;0.957)	<0.0001

Discriminative ability of phospholipid species between NSCLC and normal tissue is quantified with the AUC of the ROC-curve (95% confidence interval). *p*-value (FDR): *p*-value of MW*U* test, adapted for multiple testing.

phospholipid species based on their concordance probability estimate (CPE) with overall survival, recurrence and metastasis are listed in Supporting Information Table S5. Although some relations were detected at the 5% level, none of them remained significant after applying a correction for multiple testing (FDR). These findings confirm the ubiquitous nature of the observed changes in lipid profiles.

Discussion

Following the successes of genomics and transcriptomics, lipidomics is an emerging field in cancer biology, which promises to provide important new biological insights and has great potential towards biomarker development.[20–22] In this study, using a shotgun mass spectrometry-based platform for targeted phospholipidomics, we were able to identify 108 individual phospholipid species that significantly discriminate between NSCLC and normal tissue in a discovery set. Of these phospholipid species, 91 species were validated in a validation set. Several key changes were confirmed by 2D-imaging MS, certifying that the observed changes in lipid profiles are contributed by the cancer cells themselves and do not merely reflect changes in cell type composition. Also changes in the total abundance of specific phospholipid headgroup classes were observed. Most prominent changes included an increase in specific PIs as well as long PEs and PCs ($\geq$40 carbons in the two acyl chains together) in tumor tissue, along with a general decrease in all SMs and in multiple PS species.

These changes in phospholipid profiles are of particular interest and can be linked to well-known functions and alterations in other tumor types. PI, for instance, is known to play an important role in cancer as a source of lipid second messengers that among others activate the Akt signaling pathway. The Akt pathway is frequently activated in many cancer tissues, including NSCLC.[23] Interestingly, PI38:3, the lipid species that was most potently increased in NSCLC compared to normal tissue in this study, was recently found to be upregulated in myc-induced lymphomas,[24] along with a decrease in PS. Our parallel findings in NSCLC hence suggest that also in lung tumors these lipid species might be under the control of the *myc* gene, which is known to be amplified in NSCLC.[25,26] Along with a decrease in the content of PS in NSCLC, we observed a major decrease in the total levels of SM. Interestingly, the abundances of both SM and PS appeared to be tightly correlated. The explanation for this correlation might be found in the common serine precursor, which is required for the biosynthesis of both phospholipids, and whose concentration is known to be reduced in tumors

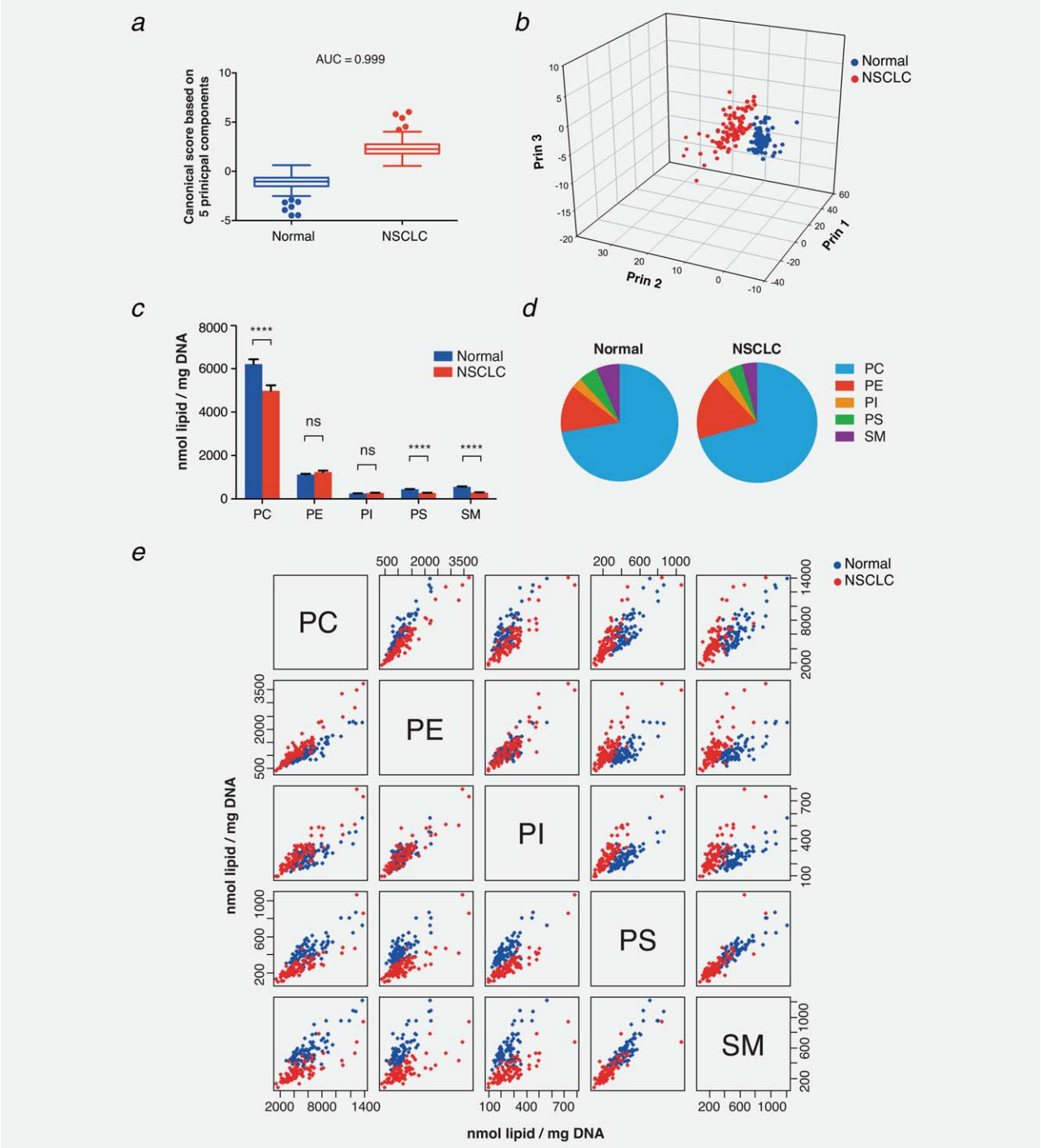

Figure 4. Phospholipid profiles discriminate NSCLC *versus* normal tissues and differential representation of phospholipid headgroup classes in NSCLC tissues *versus* normal tissues. (*a*) Phospholipid profiles from the discovery set were subjected to PCA analysis followed by LDA to distinguish NSCLC and normal tissues based on the PCA scores. The result of the PCA-LDA on the discovery set (more specifically, the canonical score from the LDA based on a specific number of principal component scores) was validated on the data in the validation set. Graph shows a validation boxplot of the canonical scores based on the solution with the lowest cross-validated misclassification error for the discovery set, that is, 5 principal components (Supporting Information Fig. S2*a*), to discriminate NSCLC versus normal tissues. (*b*) 3D-scatter plot of the principal component scores in the validation set (based on the weights from the discovery set) illustrating the discrimination between NSCLC and normal tissue. (*c*) Phospholipid species in tumor and normal tissues from 89 NSCLC patients (validation set) were summed per headgroup class (PC, PE, PI, PS and SM). Graph displays the abundance (nmol lipid/mg DNA) of different headgroup classes. Data represent mean ± standard error. **** < 0.0001; ns = not significant (MWU). (*d*) Pie charts showing relative representation of phospholipid head group classes in normal and NSCLC tissues. (*e*) Scatter plots for the abundance (nmol lipid/mg DNA) for all pairs of phospholipid headgroup classes. Relations based on 178 samples (89 NSCLC tissues in red and 89 normal tissues in blue) for any pair of PC, PE, PI, PS and SM.

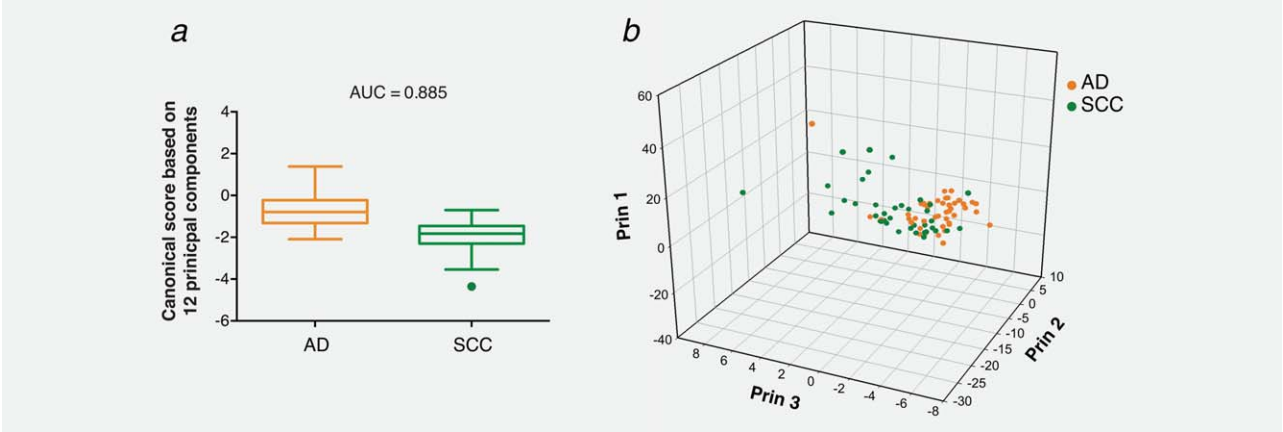

Figure 5. Phospholipid profiles discriminate AD *versus* SCC tumors. (*a*) Phospholipid profiles from the discovery set were subjected to PCA analysis followed by LDA to distinguish both subtypes based on the PCA scores. The result of the PCA-LDA on the discovery set (more specifically, the canonical score from the LDA based on a specific number of principal component scores) was validated on the data in the validation set. Graph shows a validation boxplot of the canonical scores based on the solution with the lowest cross-validated misclassification error for the discovery set, that is, 12 principal components (Supporting Information Fig. S2*b*), to discriminate AD versus SCC tumors. (*b*) 3D-scatter plot of the principal component scores in the validation set (based on the weights from the discovery set) illustrating the discrimination between NSCLC subtypes.

due to its high consumption by proliferating cells and its low abundance in the blood stream.[27] SM, which is the major sphingolipid in mammalian cells and together with cholesterol, is one of the main lipid components of lipid rafts, is known to be decreased also in other tumor cells,[28] to have an anti-cancer effect in colon cancer[29,30] and to potentiate chemotherapy.[31] In line with our results, SM42:1 and SM42:2 are decreased in proliferating/undifferentiated mammary epithelial cells, whereas PEs with 40 carbon atoms were found to be highly increased.[32]

Based on lipid profiling we not only could discriminate tumor from normal tissue, using PCA-LDA analysis we were also able to differentiate the main subtypes of NSCLC. Recently, Lee and colleagues have also shown that lipid-focused matrix-assisted laser desorption/ionization (MALDI) profiling on direct tissue sections classifies NSCLC according to the histologic type.[33] Interestingly, no major significant correlations with clinical outcome could be found, suggesting that changes in phospholipid metabolism occur early in cancer development and are a common characteristic of NSCLC cancer irrespective of the stage or aggressiveness of the tumor.

In conclusion, using a shotgun mass spectrometry based platform for targeted phospholipidomics in combination with 2D-imaging MS, we established that the phospholipid composition of NSCLC is dramatically altered compared to normal tissues. These findings may have important biological implications that warrant further investigation and may have potential for biomarker development. Besides analysis on surgical and biopsy material, the observed alterations in lipid profiles may find applications in surgery using novel tools such as the "Smart Knife," which analyzes lipids using rapid evaporative ionization mass spectrometry of the smoke made as it cuts tissue, and therefor instantly detects whether cells are cancerous or healthy by analyzing lipids.[34] Further studies will be needed to explore whether these observed changes can also be detected in the sputum or in the blood. Moreover, a more thorough analysis of the mechanisms underlying these changes will help to better understand the pathophysiology of NSCLC and may contribute to the development of new therapeutic targets.

References

1. Globocan. In: Cancer IAfRo, ed., 2012. Available at: http://globocan.iarc.fr/. (Accessed on: Sept 30, 2014).
2. Zhang Q, Li H, Jin H, et al. The global landscape of intron retentions in lung adenocarcinoma. *BMC Med Genomics* 2014;7:15
3. Tan DS, Camilleri-Broet S, Tan EH, et al. Intertumor heterogeneity of non-small-cell lung carcinomas revealed by multiplexed mutation profiling and integrative genomics. Int J Cancer 2014;135: 1092-100.
4. Lazar V, Suo C, Orear C, et al. Integrated molecular portrait of non-small cell lung cancers. *BMC Med Genomics* 2013;6:53
5. Zhang L, Zhang W, Chen K. Search for cancer risk factors with microarray-based genome-wide association studies. *Technol Cancer Res Treat* 2010;9:107–21.
6. Lane AN, Fan TW, Bousamra M, II, et al. Stable isotope-resolved metabolomics (SIRM) in cancer research with clinical application to nonsmall cell lung cancer. *Omics* 2011;15:173–82. [PMC][10.1089/omi.2010.0088] [21329461]
7. Kisluk J, Ciborowski M, Niemira M, et al. Proteomics biomarkers for non-small cell lung cancer. J Pharm Biomed Anal 2014;101:40-9.
8. Laganowsky A, Reading E, Allison TM, et al. Membrane proteins bind lipids selectively to modulate their structure and function. *Nature* 2014;510:172–5.
9. Rysman E, Brusselmans K, Scheys K, et al. De novo lipogenesis protects cancer cells from free radicals and chemotherapeutics by promoting membrane lipid saturation. *Cancer Res* 2010;70: 8117–26.
10. Swinnen JV, Van Veldhoven PP, Timmermans L, et al. Fatty acid synthase drives the synthesis of phospholipids partitioning into detergent-resistant membrane microdomains. *Biochem Biophys Res Commun* 2003;302:898–903.

11. Menendez JA, Lupu R. Fatty acid synthase and the lipogenic phenotype in cancer pathogenesis. *Nat Rev Cancer* 2007;7:763–77.
12. Scott KF, Sajinovic M, Hein J, et al. Emerging roles for phospholipase a2 enzymes in cancer. *Biochimie* 2010;92:601–10.
13. Igal RA. Stearoyl-CoA desaturase-1: a novel key player in the mechanisms of cell proliferation, programmed cell death and transformation to cancer. *Carcinogenesis* 2010;31:1509–15.
14. Visca P, Sebastiani V, Botti C, et al. Fatty acid synthase (FAS) is a marker of increased risk of recurrence in lung carcinoma. *Anticancer Res* 2004;24:4169–73.
15. Noto A, Raffa S, De Vitis C, et al. Stearoyl-CoA desaturase-1 is a key factor for lung cancer-initiating cells. *Cell Death Dis* 2013;4:e947
16. Caprioli RM, Farmer TB, Gile J. Molecular imaging of biological samples: localization of peptides and proteins using MALDI-TOF MS. *Anal Chem* 1997;69:4751–60.
17. Hankin JA, Barkley RM, Murphy RC. Sublimation as a method of matrix application for mass spectrometric imaging. *J Am Soc Mass Spectrom* 2007;18:1646–52.
18. Benjamini Y, Hochberg Y. Controlling the false discovery rate: a practical and powerful approach to multiple testing. *J R Stat Soc Ser B (Methodological)* 1995;57:289–300.
19. Gonen M, Heller G. Lehmann family of ROC curves. *Med Decis Making* 2010;30:509–17.
20. Arafah K, Longuespee R, Desmons A, et al. Lipidomics for clinical diagnosis: Dye-assisted laser desorption/ionization (DALDI) method for lipids detection in MALDI mass spectrometry imaging. *Omics* 2014;18:487–98.
21. Zhou X, Mao J, Ai J, et al. Identification of plasma lipid biomarkers for prostate cancer by lipidomics and bioinformatics. *PLoS One* 2012;7:e48889
22. Hilvo M, Denkert C, Lehtinen L, et al. Novel theranostic opportunities offered by characterization of altered membrane lipid metabolism in breast cancer progression. *Cancer Res* 2011;71:3236–45.
23. Fumarola C, Bonelli MA, Petronini PG, et al. Targeting PI3K/AKT/mTOR pathway in non small cell lung cancer. *Biochem Pharmacol* 2014;90:197–207.
24. Eberlin LS, Gabay M, Fan AC, et al. Alteration of the lipid profile in lymphomas induced by MYC overexpression. Proc Natl Acad Sci USA 2014;111:10450–55.
25. Mitani S, Kamata H, Fujiwara M, et al. Analysis of c-myc DNA amplification in non-small cell lung carcinoma in comparison with small cell lung carcinoma using polymerase chain reaction. *Clin Exp Med* 2001;1:105–11.
26. Hammerman PS, Lawrence MS, Voet D, et al. Comprehensive genomic characterization of squamous cell lung cancers. *Nature* 2012;489:519–25.
27. Medina MA Marquez J, Nunez de Castro I. Interchange of amino acids between tumor and host. *Biochem Med Metab Biol* 1992;48:1–7.
28. Barcelo-Coblijn G, Martin ML, de Almeida RF, et al. Sphingomyelin and sphingomyelin synthase (SMS) in the malignant transformation of glioma cells and in 2-hydroxyoleic acid therapy. *Proc Natl Acad Sci USA* 2011;108:19569–74.
29. Dillehay DL, Webb SK, Schmelz EM, et al. Dietary sphingomyelin inhibits 1,2-dimethylhydrazine-induced colon cancer in cf1 mice. *J Nutr* 1994;124:615–20.
30. Lemonnier LA, Dillehay DL, Vespremi MJ, et al. Sphingomyelin in the suppression of colon tumors: prevention versus intervention. *Arch Biochem Biophys* 2003;419:129–38.
31. Modrak DE, Lew W, Goldenberg DM, et al. Sphingomyelin potentiates chemotherapy of human cancer xenografts. *Biochem Biophys Res Commun* 2000;268:603–6.
32. Doria ML, Ribeiro AS, Wang J, et al. Fatty acid and phospholipid biosynthetic pathways are regulated throughout mammary epithelial cell differentiation and correlate to breast cancer survival. Faseb J 2014;28:4247–64.
33. Lee GK, Lee HS, Park YS, et al. Lipid MALDI profile classifies non-small cell lung cancers according to the histologic type. *Lung Cancer* 2012;76:197–203.
34. Balog J, Sasi-Szabo L, Kinross J, et al. Intraoperative tissue identification using rapid evaporative ionization mass spectrometry. *Sci Transl Med* 2013;5:194ra9.